ANTIOXIDANTS & REDOX SIGNALING
Volume 18, Number 7, 2013

DOI: 10.1089/ars.2012.4591

Discoveries

ORIGINAL RESEARCH COMMUNICATION

Selenium Inhibits Renal Oxidation and Inflammation But Not Acute Kidney Injury in an Animal Model of Rhabdomyolysis

Anu Shanu,[1] Ludwig Groebler,[1] Hyun Bo Kim,[1] Sarah Wood,[1] Claire M. Weekley,[2] Jade B. Aitken,[3] Hugh H. Harris,[2] and Paul K. Witting[1]

Abstract

Acute kidney injury (AKI) is a manifestation of rhabdomyolysis (RM). Extracellular myoglobin accumulating in the kidney after RM promotes oxidative damage, which is implicated in AKI. ***Aim:*** To test whether selenium (Se) supplementation diminishes AKI and improves renal function. ***Results:*** Dietary selenite increased Se in the renal cortex, as demonstrated by X-ray fluorescence microscopy. Experimental RM-stimulated AKI as judged by increased urinary protein/creatinine, clusterin, and kidney injury molecule-1 (KIM-1), decreased creatinine clearance (CCr), increased plasma urea, and damage to renal tubules. Concentrations of cholesterylester (hydro)peroxides and F_2-isoprostanes increased in plasma and renal tissues after RM, while aortic and renal cyclic guanidine monophosphate (cGMP; marker of nitric oxide (NO) bioavailability) decreased. Renal superoxide dismutase-1, phospho-P65, TNFα gene, MCP-1 protein, and the 3-chloro-tyrosine/tyrosine ratio (Cl-Tyr/Tyr; marker of neutrophil activation) all increased after RM. Dietary Se significantly decreased renal lipid oxidation, phospho-P65, TNFα gene expression, MCP-1 and Cl-Tyr/Tyr, improved NO bioavailability in aorta but not in the renal microvasculature, and inhibited proteinuria. However, CCr, plasma urea and creatinine, urinary clusterin, and histopathological assessment of AKI remained unchanged. Except for the Se++ group, renal angiotensin-receptor-1/2 gene/protein expression increased after RM with parallel increases in MEK1/2 inhibitor-sensitive MAPkinase (ERK) activity. ***Innovation:*** We employed synchrotron radiation to identify Se distribution in kidneys, in addition to assessing reno-protection after RM. ***Conclusion:*** Se treatment has some potential as a therapeutic for AKI as it inhibits oxidative damage and inflammation and decreases proteinuria, albeit histopathological changes to the kidney and some plasma and urinary markers of AKI remain unaffected after RM. *Antioxid Redox Signal.* 18, 756–769.

Introduction

Up to 53% of patients with severe burns develop rhabdomyolysis (RM) (33, 46). Acute kidney injury (AKI) is a clinical complication of RM and this is associated with ~5% mortality in this group of patients (9). The pathogenesis of RM is initiated by sarcolemmic injury that stimulates calcium influx into muscle cells. Subsequent muscle myolysis releases extracellular myoglobin (Mb) that accumulates in the kidney (8). In humans, RM is characterized by increased serum creatinine, creatine kinase, lactate dehydrogenase, electrolyte imbalances, hyperuricaemia, and aciduria with pigmenturia (8, 23, 30). Myoglobin solubility decreases in acidic conditions, facilitating its precipitation in renal tubules (65): co-precipitation of Mb with Tamm–Horsfall protein yields renal casts (65). Extracellular Mb can promote renal lipid oxidation (21, 23, 32) and decrease thiol redox status in kidney epithelial cells (49). Iron chelators can attenuate oxidative damage, indicating that iron-induced oxidative stress is a feature of RM (9, 22, 37).

Limiting nitric oxide (NO) bioavailability due to NO scavenging and/or oxidation by (oxy)Mb, promotes vasoconstriction (3, 8, 43). Vasoconstrictive F_2-isoprostanes generated through radical-mediated arachidonic acid oxidation may also affect vascular tone (44). Furthermore, activation of

[1]Discipline of Pathology, Redox Biology Group, Bosch Institute, and [3]School of Chemistry, The University of Sydney, Sydney, Australia.
[2]School of Chemistry and Physics, The University of Adelaide, Adelaide, Australia.

Innovation

The link between oxidative stress and acute renal injury after rhabdomyolysis is based on antioxidants ameliorating oxidative damage and improving renal function in animal models. We have supplemented rats with the trace element selenium and employed cutting-edge synchrotron radiation techniques to confirm increased Se distribution in renal tissues before the assessment of reno-protection, using a combination of traditional and contemporary biomarkers of renal damage and inflammation. Our data indicate that Se supplementation inhibits renal oxidative damage, inflammation, and proteinuria resulting from experimental rhabdomyolysis, yet histopathological changes and some markers of acute kidney injury remain unaffected.

the renin–angiotensin system, which releases angiotensin II (AngII), also stimulates vasoconstriction (16), which decreases glomerular perfusion. Clinical management of AKI includes administration of sodium bicarbonate to normalize acidic urine, and mannitol, an osmotic diuretic, although some clinical studies show no benefit on mortality (8).

In the kidney, the actions of AngII are mediated by binding to angiotensin receptor I (ATRI) with subsequent phosphorylation of mitogen-activated protein kinases (MAPK), which are implicated in hypertension and chronic kidney disease (24). In addition to vasoconstriction, AngII increases oxidative stress and production of monocyte chemoattractant protein-1 (MCP-1) through activating nuclear factor kappa beta (NFκB) in proximal epithelial and glomerular mesangial cells (46, 55). Oxidative stress is implicated in promoting renal ATRI gene expression, leading to sodium retention and increased blood pressure (7).

Selenium (Se) is a trace element present in the active site of selenoproteins as a unique selenocysteine residue (42). The selenoenzyme glutathione peroxidase-1 (GPx-1) degrades low-molecular weight hydroperoxides and maintains cellular redox balance. Its affinity for H_2O_2 is greater than catalase, making it an efficient antioxidant (60). It is also the most Se-sensitive selenoprotein, making it a good marker for intrinsic selenium status (51). Our study aims to investigate the impact of Se supplementation on markers for AKI following experimental RM.

Results

Consistent with our previous studies (23, 32), 24 h after administration of hypertonic glycerol (50% v/v in saline), histological examination of the hind leg muscle demonstrated the presence of edema and intramuscular hemorrhage with evidence of pyknotic nuclei, indicative of severe muscle myolysis (Supplementary Fig. S1a–c; Supplementary data are available online at www.liebertonline.com/ars). Extracellular Mb was also present in the circulating plasma of animals treated with hypertonic glycerol (Supplementary Fig. S1d), and the total globin concentration in samples of urine collected over the 24 h was similar across all glycerol-treated groups and significantly greater than that detected in urine from the sham group (where sterile saline was administered in place of glycerol) (Supplementary Fig. S1e).

Tissue Se distribution

X-ray fluorescence microspectroscopy (XFM) was used to map the distribution and to determine Se concentration in tissues from sham, RM (glycerol-treated) and Se++ (dietary Se 5 ppm) groups that were sectioned (thickness 30 μm), and dehydrated onto silicon nitride (see Methods). The Se and K^+ elemental distribution and a corresponding hematoxylin and eosin-stained section from the same (Se++) sample are shown (Fig. 1A). The distribution of K^+ was uniform across all kidney regions, as expected for this ubiquitous cation. The majority of Se was concentrated within the renal cortex and to a

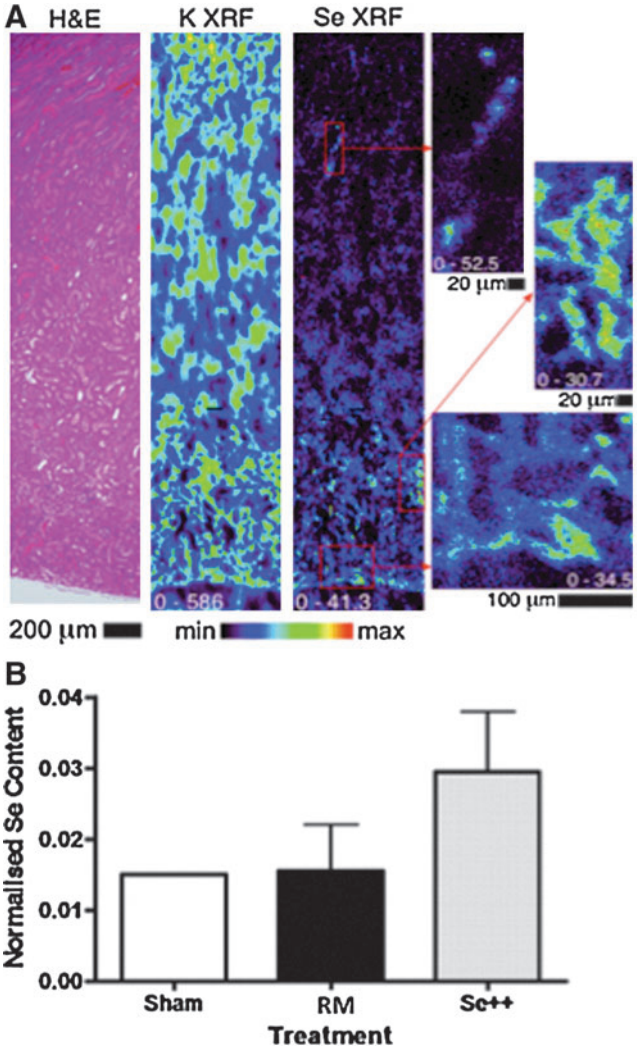

FIG. 1. X-ray fluorescence imaging reveals renal K^+ and Se distribution. Animals were supplemented with 5 ppm dietary Se (Se++ group) as described in the Methods section. Kidneys were harvested 24 h after experimental RM (except the sham), frozen sections were obtained and applied to silicon nitride windows and incubated under vacuum (<0.02 Torr; 12 h) before transport to the Australian Synchrotron for assessment by XFM imaging. **(A)** The elemental distribution of Se and potassium ions were then determined by elemental mapping, and representative data is reported for tissue from a rat in the Se++ group together with a parallel renal section stained with hematoxylin and eosin. **(B)** Quantification of Se reported as area normalized density units. Images are representative of at least three different microscopic fields from $n=2$ kidneys.

Table 1. Plasma and Kidney Levels of Native and Oxidized Lipids and Vitamin E Before and After Experimental Rhabdomyolysis

	*[UC] m*M	*[TOH]* μM	*[CEO(O)H] n*M	*[C20:4] m*M	*[C18:2] m*M	*[F_2-isoprotanes] pg/mL*
Plasma						
Sham	0.9 (0.2)	7.8 (1.8)	10.1 (3.2)	1.2 (0.3)	0.3 (0.2)	28.6 (4.8)
RM	0.8 (0.3)	6.4 (1.3)	46.3 (9.6)*	0.9 (0.8)	0.2 (0.1)	121.3 (18.3)*
Se+	0.9 (0.3)	8.1 (2.8)	24.6 (3.2)*#	1.4 (0.7)	0.4 (0.2)	53.6 (5.7)*#
Se++	0.8 (0.2)	7.0 (1.9)	19.9 (4.1)*#	1.2 (0.3)	0.4 (0.1)	48.9 (6.2)*#
	[UC] nmol/mg P	*[TOH] pmol/mg P*	*[CEO(O)H] pmol/mg P*	*[C20:4] nmol/mg P*	*[C18:2] nmol/mg P*	*[F_2-isoprotanes] pg/mg P*
Kidney tissues						
Sham	127.6 (27.7)	433.1 (159.3)	0.3 (0.2)	0.8 (0.3)	0.05 (0.03)	33.8 (6.7)
RM	115.2 (64.8)	426.1 (195.6)	7.9 (3.5)*	0.6 (0.5)	0.04 (0.03)	227.2 (35.5)*
Se+	104.0 (67.2)	347.5 (137.0)	4.0 (2.9)*#	0.8 (1.0)	0.03 (0.05)	97.8 (22.7)*#
Se++	118.5 (36.8)	442.9 (153.1)	4.5 (2.7)*#	0.5 (0.4)	0.04 (0.04)	77.2 (26.2)#

The lipids from plasma and homogenized renal samples were extracted and analyzed by liquid chromatography as described in the Methods section. Levels of unesterified cholesterol (UC), vitamin E (as α-tocopherol; TOH), cholesteryl arachidonate (C20:4), cholesteryl linoleate (C18:2) together referred to as cholesteryl esters (CE), cholesterylester hydroperoxides and hydroxides (CEO(O)H) and concentrations of 8-epi-F_2-isoprostane were determined across sham, RM and Se-supplemented groups. Data represents mean ± (SD); plasma and kidneys from 6 rats, except for F_2-isoprostane analysis in the kidneys where 4 rats were used.

*Different to the sham; $P < 0.001$.

#Different to the RM group; $P < 0.05$.

lesser extent the renal medulla (*c.f.*, XFM and parallel H&E-stained images, Fig. 1A). Dietary Se (at 5 ppm) increased both renal Se levels ~2-fold (Fig. 1B) and circulating GPx activity ~1.5 ± 0.1-fold (mean ± SD; $n = 4$) compared to the corresponding sham (Supplementary Fig. S2).

Oxidative damage to the kidney

Levels of unesterified cholesterol (UC), vitamin E (as α-tocopherol; α-TOH), cholesteryl arachidonate (C20:4), and cholesteryl linoleate (C18:2), together referred to as cholesteryl esters (CE), were unchanged in all groups (Table 1). Lipid peroxidation increased markedly in both plasma and renal tissues after RM, as judged by comparing concentrations of cholesteryl ester-derived lipid hydro(per)oxides (CE-O(O)H; a marker of cell membrane oxidation) and F_2-isoprostanes (marker of polyunsaturated fatty acid oxidation) determined in the sham and RM groups. By contrast, Se supplementation decreased CE-O(O)H and F_2-isoprostane accumulation in both the plasma and renal tissues, although this did not reach the corresponding baseline concentrations determined in the sham (Table 1).

Urinary and plasma markers of AKI

Urinary clusterin, a marker for AKI that correlates with hypoxic tubular damage (28), and kidney injury molecule-1 (KIM-1), a glycoprotein released in the event of early proximal tubule injury (6, 59, 61), both increased significantly after RM (Fig. 2A and 2B). While urinary clusterin was unaffected by Se supplementation, KIM-1 decreased significantly in the Se++ group (*vs.* the RM group), although it remained elevated by comparison to the sham. Both urinary protein and the ratio of protein:creatinine increased significantly in all glycerol-treated animals, except in the Se++ group, where lower levels of proteinuria (and the corresponding protein:creatinine ratio) were indicative of reno-protection (Table 2). A marked decrease in the value of body weight normalized creatinine clearance (CCr) was determined after experimental RM (Table 2) and this was unaffected by Se supplementation. Almost all plasma biochemical markers were unchanged after experimental RM except blood urea nitrogen (BUN) and plasma creatinine, which increased in all animals after RM irrespective of Se supplementation (Table 2).

Vascular function

Binding of NO to its molecular target, soluble guanylyl cyclase, activates cGMP production (56). Induction of experimental RM yielded significantly lower cGMP levels than detected in the aorta (Fig. 3A) and kidney (Fig. 3B) from the sham group. Dietary Se supplementation restored cGMP content in the thoracic aortic to similar levels detected in the sham, indicating an improved vascular tone in large bore aortic vessels after experimental RM (Fig. 3A). By contrast, Se did not restore renal cGMP, with levels remaining similar to the RM group irrespective of the level of Se supplementation (Fig. 3B). These data indicate that, while Se enhanced vascular function in large arterial vessels, renal microvascular dysfunction remained unaffected.

Changes to gene expression and proteins after experimental RM

Gene expression of the antioxidant response elements (Cu-Zn)SOD-1, (Mn)SOD-2, and GPx-1 increased significantly after RM (Table 3). In case of SOD-1, RM stimulated an accumulation of monomeric and dimeric SOD-1 in renal tissues. This was marginally inhibited by dietary Se supplementation, with decreases in the active dimeric SOD evident in both the Se+ and Se++ groups (Fig. 4A). Consistent with this evaluation of protein accumulation, immunoactive SOD increased in tubule epithelial cells in all glycerol-treated groups (Supplementary Fig. S3A(i–iv)). Accumulation of SOD-1 was primarily in the renal

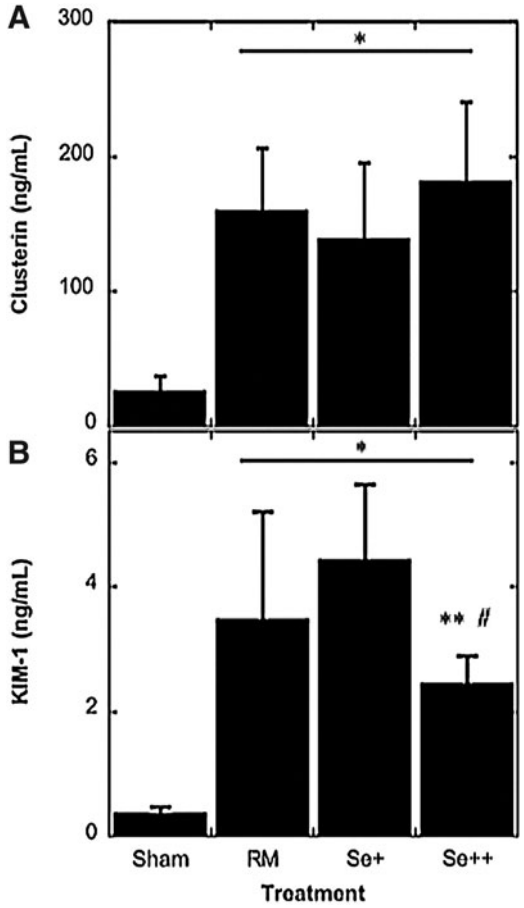

FIG. 2. Urinary markers of AKI after experimental RM. Animals were treated as described in the legend to Figure 1 before inducing experimental RM (except the sham) for a 24 h period during which urine was collected prior to harvest of blood and kidneys. Urinary concentrations of **(A)** clusterin (ng/ml) and **(B)** KIM-1 (ng/ml) were measured with a commercial Luminex assay. Data are expressed as mean ± SD; $n = 4$ or $n = 6$ for clusterin and KIM-1, respectively. *Different to the sham; $p < 0.05$. #Different to the RM group; $p < 0.05$; **Different to the RM and Se+ group; $p < 0.01$.

tubule epithelia of the cortex and outer medullar regions—some weak staining was evident within glomeruli (compare insets in Supplementary Fig. S3A(i–iv)). Despite increases in renal SOD-1 after RM, total SOD activity showed only a weak trend to increase after RM (Fig. 4B) and this was ameliorated with Se supplementation, albeit this did not reach statistical significance.

Gene expression for GPx-1 remained high in all glycerol-treated animals irrespective of Se supplementation (Table 3), and this resulted in weak increases in the renal content of GPx-1 protein in glycerol-treated animals as judged by Western blotting (Fig. 4C). By contrast, immunohistochemical assessment of GPx-1 (Supplementary Fig. S3B[i–iv]) showed similar levels of GPx-1 staining (localized to tubular epithelia and parietal epithelia lining Bowman's capsule) in all treatment groups. Unexpectedly, total GPx activity diminished after RM and, although Se supplementation improved tissue GPx activity, it remained below that determined in the sham (Fig. 4D). It is notable that Mb (present in the renal tissues after RM) also exhibits peroxidase-like activity (43) and this may interfere with *ex vivo* determinations of renal GPx activity relative to the sham samples that lack extracellular Mb.

Gene expression for the redox-sensitive transcription factor NFκB was unchanged 24 h after RM induction (Table 3). However, phosphorylation of the p65 subunit increased in response to RM (Fig. 4E) and this occurred concomitantly with enhanced gene expression of pro-inflammatory TNFα (Table 3) and increased levels of MCP-1 in both circulating plasma and renal tissues (Fig. 4F and 4G, respectively). Se supplementation decreased P65 phosphorylation, and at the highest dose, Se attenuated TNFα gene expression and MCP-1 accumulation in renal tissues, although plasma MCP-1 remained unaffected.

Neutrophil stimulation leads to the production of hypochlorous acid that oxidizes and chlorinates proteins including Mb (52). Monitoring the level of 3-chloro-tyrosine provides a useful index of tissue inflammation (26). Induction of experimental RM markedly increased the 3-chloro-tyrosine/tyrosine ratio as determined by quantitative mass spectrometry (Fig. 5A). Consistent with Se inhibiting inflammation, the 3-chloro-tyrosine/tyrosine ratio decreased significantly in Se supplemented animals and this reached significance at the highest Se dose administered (Fig. 5A).

Interestingly, the extent of plasma protein chlorination equated to ~7% of the available pool of protein tyrosine, well above levels previously reported. One possible explanation for increased protein chlorination is that administration of hypertonic glycerol to the hind leg muscle induces a local inflammatory response that generates chlorinated proteins, including chloro-Mb. Release of chloro-Mb into the circulation, combined with the rapid clearance of extracellular Mb to the kidney, may account in part for the 3-chloro-tyrosine/tyrosine ratio determined in the renal tissues after RM. To assess this possibility, we determined the levels of 3-chloro-tyrosine in plasma before and after immunoprecipitation of Mb. Overall, RM markedly increased plasma levels of 3-chloro-tyrosine (Fig. 5B). A comparison of 3-chloro-tyrosine content in the RM group before immunoprecipitation (RM), the residual supernatant (RMIPS), and the precipitate (RMIP) indicated that the level of 3-chloro-tyrosine in plasma decreased significantly by ~70% after immunoprecipitation of Mb. Supplementation with Se at 5 ppm in the diet significantly decreased the plasma content of 3-chloro-tyrosine (Fig. 5B), consistent with the anti-inflammatory action of this essential micronutrient documented here (Fig. 4E–4G).

Kidney histology

Kidneys from the sham displayed normal tubular epithelia in the renal cortex, unobstructed tubules, and unremarkable glomeruli containing thin-walled capillaries within the glomerular tuft (Fig. 6). Consistent with RM inducing an increase in KIM-1, glycerol treatment yielded tubule epithelial necrosis, thickening and disruption/displacement of the tubular epithelium with evidence of cast material, irrespective of Se status (Fig. 6A, with 6B–6D). After RM, glomeruli appeared congested and the capillaries within the tuft were more difficult to identify due to the presence of relatively more nuclear staining than evident in the corresponding sham samples. The latter may indicate either cellular infiltration or mesangial proliferation stimulated by the elevated levels of

Table 2. Plasma and Urinary Biochemistry

Parameter	*Sham* (n = *8*)	*Urine RM* (n = *7*)	*Se+* (n = *9*)	*Se++* (n = *6*)
Na^+ (10^{-3} *M*)	48.3 (29.7)	50 (12.5)	29.4 (20.2)	22.8 (17.6)
K^+ (10^{-3} *M*)	147.9 (60.9)	137.4 (24.38)	118.5 (21.8)	110.7 (66.4)
Body weight normalized CCR (ml/min/kg)	12.7 (2.8)	4.3 (0.2)*	3.6 (5.7)*	5.5 (3.5)*
Protein (mg/ml)	2.1 (1.9)	9.5 (3.5)*	7.8 (2.5)*	3.0 (2.2)#
Protein:creatinine	0.05 (0.04)	0.19 (0.06)*	0.15 (0.04)*	0.07 (0.05)#
		Plasma		
Na^+ (10^{-3} *M*)	188.8 (52.5)	170.7 (49.1)	213 (45.9)	209.3 (70.1)
K^+ (10^{-3} *M*)	3.9 (1.2)	4.3 (0.9)	3.2 (0.3)	2.6 (1.2)
Cl^- (10^{-3} *M*)	119.4 (17.9)	106.7 (18.8)	103.9 (2.8)	74.6 (46.2)
Urea (10^{-3} *M*)	5.3 (1.0)	14.8 (5.2)*	19.4 (5.6)*	14.6 (5.9)*
Creatinine (10^{-6} *M*)	16.7 (12.7)	63.3 (17.9)*	88.6 (18.4)*	56.2 (12.2)*
Ca^{2+} (10^{-3} *M*)	2.2 (0.4)	2.1 (0.6)	1.8 (0.4)	1.4 (0.5)

Blood plasma and urine were collected 24 h after the induction of experimental RM and concentrations of different biochemical parameters were measured. Data expressed as Mean ± (SD). Units of measurement and the numbers of samples tested (*n* values for all parameters) are as indicated in the table. Creatinine clearance (CCR) was calculated as described in the Methods section.

*Different to the sham group; $p < 0.05$.

#Different to RM and Se+ groups; $p < 0.05$.

For comparison, normal plasma ranges for Na^+ (138–152), K^+ (3.7–4.7), Cl^- (100–105), and Ca^{2+} (2.4–2.6) $\times 10^{-3}$ *M* in the male Sprague Dawley rat are shown as derived from References 18, 20, and 35.

renal MCP-1 and NFκB activation (Fig. 4G), which may be linked to the increase in the 3-chloro-tyrosine/tyrosine ratio determined in the corresponding renal homogenates (Fig. 5A).

Angiotensin receptors

Gene expression of ATR I/II increased across all groups relative to the sham. This relative increase was ameliorated by Se supplementation; however, expression remained greater than that detected in the sham (Table 3). Parallel increase in immunoactive ATRI after RM was detected in the glomerular capillary network and in the epithelium lining the renal tubules in all groups after RM (Fig. 7). A similar pattern of enhanced protein expression was detected for ATRII (not shown), suggesting that upregulation of ATR I/II receptors facilitates the function of vasoactive AngII.

Renal kinase activity

Renal vasoconstriction is attributed to AngII binding to ATRI to enhance MAPK activity through kinase phosphorylation. MAPKinase activity increased significantly after RM and this was sensitive to MEK-1/2 inhibition. MAPKinase activity remained elevated in the Se+ group, but was decreased to similar levels determined for the sham in the Se++ group (Fig. 8). Consistent with this documented increase in MAPK activity after RM, immunoactive p-p38 (Fig. 9A) and p-ERK1/2 (Fig. 9B) increased after RM and the proteins were distributed primarily in the tubule epithelia and glomeruli similar to ATRI/ATRII. The extent of p-p38 and p-ERK1/2 staining in renal tissues was largely unaffected by Se supplementation, even though ERK kinase activity was shown to be inhibited in the Se++ group.

Discussion

Several clinical strategies have been adopted to prevent AKI following RM. The current consensus is that RM-mediated AKI occurs through a pathogenic mechanism involving oxidative stress, tubular cast formation, vasoconstriction, and renal inflammation (8). Oxidative stress manifests as an accumulation of oxidized lipids, depletion of endogenous antioxidants, and activation of pro-inflammatory pathways. Variable reno-protective outcomes have been reported for different natural (5, 15, 23, 58) and synthetic antioxidants (32, 40) in animal models of RM. However, large-scale therapeutic interventions with antioxidants in humans have not been reported.

Selenium is a micronutrient that has been implicated in improved defense against oxidative stress and immunity. Dietary recommendations for Se are based on optimal GPx activity *in vitro* (4): 55–60 μg for adults, with an upper limit of 400 μg (Nutrient Reference Values: Australia & New Zealand, 2005) above which Se is considered toxic. Studies examining Se supplementation or Se deficiency in a rat model of deep tissue burn demonstrated that Se can restore total antioxidant status through improving total GPx activity, yet it does not reverse oxidative tissue damage (46), which is potentially a critical factor in the pathogenesis of AKI. Our study confirms that Se supplementation improves the kidney redox status (inhibiting CE-O(O)H and F_2-isoprostane accumulation) and diminishes inflammation (inhibiting NFκB activation, TNFα gene expression, and MCP-1 production in renal tissues). This activity decreases renal levels of chlorinated protein, although the latter may in part involve Se limiting the local inflammatory response in the hind leg muscle after glycerol administration. Urinary KIM-1 also decreased at the highest Se dose administered consistent with inhibition of epithelial cell de-differentiation in response to proximal tubular injury. However, while supplemented Se preserves vascular function in low-resistance arteries, it is unable to preserve NO bioavailability in the renal microvasculature or inhibit RM-mediated renal dysfunction assessed by monitoring CCR and plasma creatinine or BUN.

Elemental XFM mapping of kidney tissues revealed that Se increases ~2-fold with supplementation (Fig. 1A) and that Se is primarily distributed in the cortical regions. After

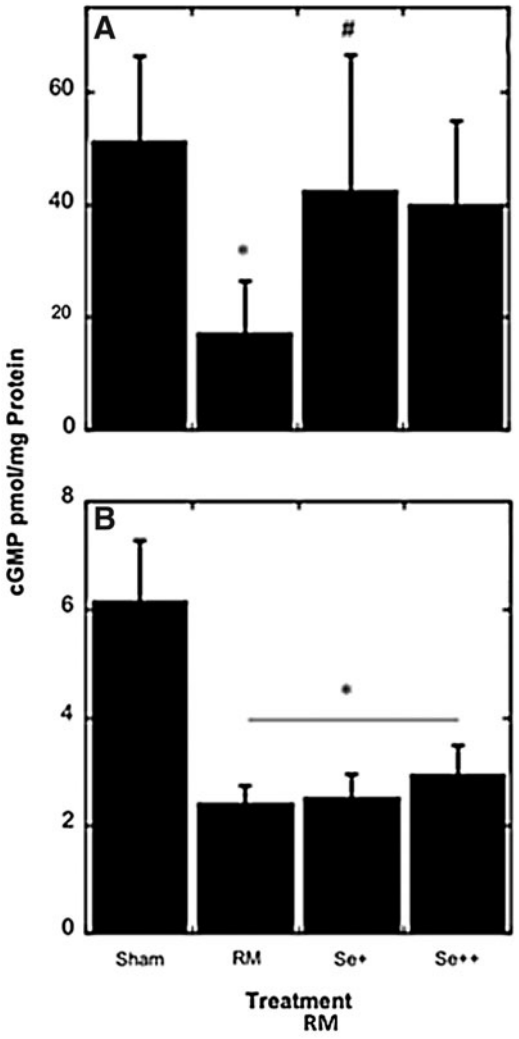

FIG. 3. Aortic and renal levels of cGMP after experimental RM. Animals were treated as described in the legend to Figure 1 before inducing experimental RM (except the sham). After 24 h, **(A)** aortae and **(B)** kidneys were harvested, homogenized, and cGMP assessed with a commercial kit as described in the Methods section. Data are expressed as mean ± SD; $n = 6$ samples from different animals. *Different to the sham; $p < 0.01$. #Different to the RM group; $p < 0.05$.

experimental RM, gene expression of renal GPx-1 increases; however it is not clear if this led to corresponding increases in GPx-1 protein or activity in the same renal tissues (see Fig. 4C and D; Supplementary Fig. 3B(i–iv)). Expression of GPx-1 in the renal tubules may be a response to pro-oxidant Mb that is deposited in tubular casts (11), which initiates the expression of antioxidant response elements (Table 4) in the tubule epithelia. Consistent with GPx-1 localization to tubule epithelia, a recent high-resolution imaging study demonstrated endogenous Se was associated with GPx-3 in the tubule epithelia, although this was in the absence of RM (34). The renal antioxidant response to insult is confirmed by increases in the accumulation of SOD-1 in tubular epithelia after RM (Fig. 4A and Supplementary Fig. 3A(i–iv)), although this did not yield an increase in SOD-1 activity in the corresponding renal homogenate (Fig. 4B).

A parallel increase in GPx-1 gene expression was demonstrated in all RM groups. However, as shown here and elsewhere (1), increased GPx-1 gene expression is not consistently associated with increased protein activity. Interestingly, increased GPx activity was demonstrated in circulating blood from Se-supplemented animals. Therefore, renal tissues and cells may not be protected against sustained superoxide radical anion/H_2O_2 generation unless circulating GPx-1 or renal catalase activity is able to metabolize any accumulating low-molecular weight peroxides. Notably, low-molecular weight peroxides react with hemoproteins (such as Mb) to yield pro-oxidative species that can damage biological lipids (9) and this may account for the increases in CE-O(O)H and F_2-isoprostanes in the plasma and renal tissues after RM determined here (Table 1) and elsewhere (9, 23, 32).

Although Se inhibited CE-O(O)H and F_2-isoprostane accumulation in plasma and renal tissues, concentrations of oxidized lipids generally remained higher than in the sham, which manifests as renal oxidative stress. The latter activates redox sensitive NFκB to initiate transcription of pro-inflammatory TNFα and MCP-1 (46). Decreased glomerular perfusion as a result of tubular cast formation may also stimulate transient renal hypoxia that activates NFκB (13). In animals supplemented with 5 ppm Se, activation of NFκB and upregulation in pro-inflammatory TNFα decreased significantly after experimental RM (Table 3), indicating that dietary Se can attenuate renal inflammation. Consistent with this observation, Se supplementation inhibited the accumulation of MCP-1 in renal tissues (not plasma), and this was linked to decreases in the renal content of chlorinated proteins, urinary KIM-1, and the extent of proteinuria (either absolute or creatinine normalized) at least for the highest Se dose tested (Table 2). Despite these positive outcomes, body-weight adjusted CCr, BUN, levels of urinary clusterin, and histopathological assessment remained largely unaffected 24 h after induction of RM in this Se-supplemented group. At least in the case for clusterin, continued secretion of this protein irrespective of Se status may be linked to a role in apoptosis suppression in renal tissues (45).

Our data demonstrated a diminished NO bioavailability/bioactivity after induction of RM in both large-bore vessels and the microvasculature of the kidney. While Se protected low-resistance arteries from vascular dysfunction, the microvasculature of the kidney remained impaired as judged by comparing levels of renal cGMP between RM and Se-treated animals. Interestingly, Se supplementation inhibited the accumulation of F_2-isoprostanes in both renal tissues and plasma (Table 2). This oxidation product is implicated in vasoconstriction (43). Therefore, inhibiting F_2-isoprostane production in the kidney is unlikely to be a useful strategy to restore vascular NO bioactivity in the renal microvasculature after RM, as other factors are likely more important in assessing potential therapeutic targets. For example, levels of plasma uric acid have been suggested as a marker for mortality in humans with AKI (33), although the available evidence suggests that Se does not affect uric acid metabolism (36).

Angiotensin II is a powerful regulator of renal vascular tone. Binding of AngII to ATRI/II receptors elicits multiple pathways that manifest as decreased renal blood flow and Na^+ excretion (25). Inhibitor studies indicate that AngII-stimulated phosphorylation of ERK and p38 MAPKs initiates

Table 3. Relative Gene Expression in Renal Tissues Before and After Experimental Rhabdomyolysis

	SOD-1	*SOD-2*	*GPx 1*	*NFκB*	*TNFα*	*ATR I*	*ATR II*
Sham	1.0 (0.1)	1.0 (0.0)	1.0 (0.0)	1.0 (0.1)	1.0 (0.0)	1.0 (0.0)	1.0 (0.0)
RM	2.1 (0.1)*	7.1 (1.1)*	2.4 (2.2)*	1.0 (0.2)	15.7 (4.4)*	13.1 (4.1)*	13.3 (5.5)*
Se+	2.7 (0.4)*	4.7 (1.1)*#	3.7 (2.5)*	1.9 (0.2)	17.9 (5.8)*	7.0 (1.7)*#	13.4 (5.6)*
Se++	1.3 (0.4)**	2.1 (0.4)**#	2.3 (0.9)*	0.8 (0.4)	8.4 (3.2)	7.0 (1.6)*#	6.9 (2.3)*

Gene regulation studies were performed as described in the Methods section. Data are expressed as mean ± (SD); $n = 6$ for sham, RM, Se+, and Se++ groups. Antioxidant stress elements (SOD-1/2 and GPx-1), inflammation markers (TNF and NFκB), and receptors for angiotensin (ATRI and ATRII) were measured and normalized against the corresponding β-actin housekeeping gene. Each treatment group was then expressed as a fold-change compared to the sham (arbitrarily assigned unitary value).

*Different to the sham; $p < 0.01$.

#Different to the RM group; $p < 0.05$.

**Different to the Se+ group; $p < 0.05$.

oxidative stress (29, 55), MCP-1 activation via the NFκB pathway (53), and endothelial dysfunction (decreased NO bioavailability (57)); all features of this study. Although dietary Se (5 ppm selenium as sodium selenite) inhibited oxidative damage, reduced renal inflammation, and significantly ameliorated renal MAPKinase activity, this did not impact on the extent of ATRI/II receptor expression, the phosphorylation of ERK and P38 (assessed by immunohistochemistry) or completely restore renal function as judged by comparing the traditional markers CCr, BUN, and tissue histopathology. Inhibitor studies implicate ATRI in promoting renal injury through production of reactive oxygen species, whereas ATRII is most commonly linked to reno-protection (25). The inability for Se to regulate ATRI/II accumulation in the kidney suggests AngII-stimulation of renal insufficiency may be independent of the reno-protection provided by supplemented

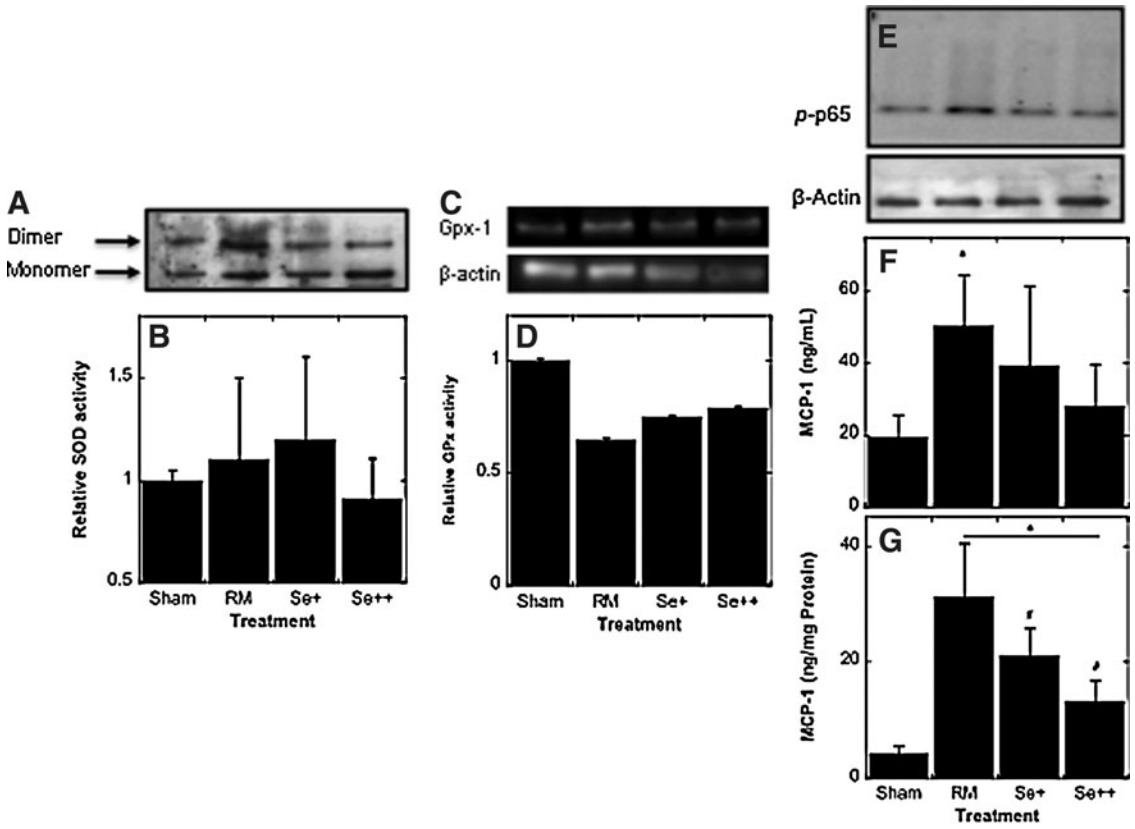

FIG. 4. Accumulation of SOD-1, GPx-1, and phosphorylated P65 and corresponding protein activities in the kidney after experimental RM. Animals were treated as described in the legend to Figure 1 before inducing experimental RM (except the sham). Animals were sacrificed, and blood and kidneys were harvested to prepare plasma and renal homogenates as described in the Materials and Methods section. Homogenate proteins were separated on SDS-PAGE and immunostained for **(A)** SOD-1 protein and **(B)** corresponding activity was assessed; **(C)** GPx-1 and **(D)** corresponding activity and **(E)** p-P65 and actin as loading control; MCP-1 levels in **(F)** plasma and **(G)** renal tissues. Enzyme activity is expressed as a fold-change relative to the activity determined for the sham. Levels of MCP-1 were determined using a commercial EIA. Data are expressed as mean ± SD; $n = 3$ (SOD and GPx) or $n = 4$ (p-p65 and MCP-1) independent experiments using renal and plasma samples from different animals. *Different to the sham; $p < 0.01$. #Different to the RM group; $p < 0.05$.

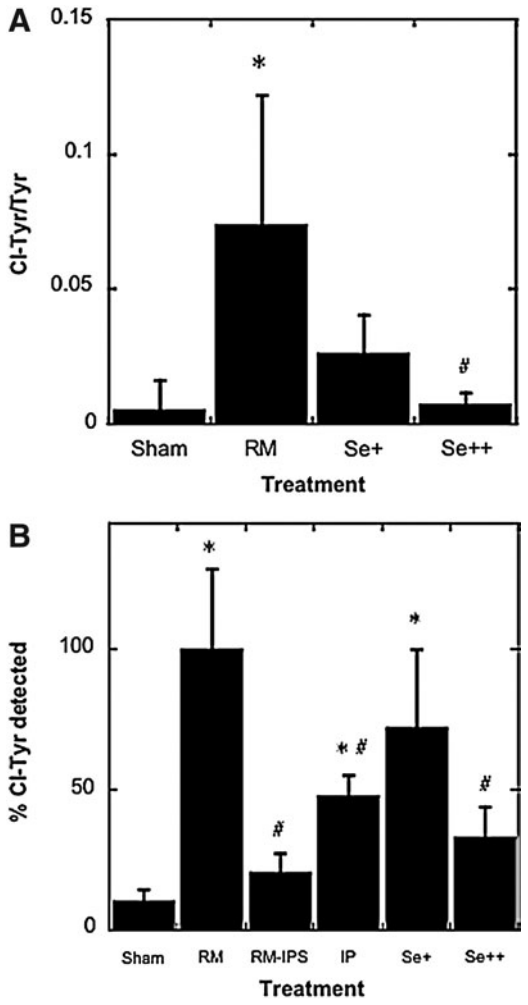

FIG. 5. Impact of RM on the renal and plasma content of 3-chlroro-tyrosine. Animals were treated as described in the legend to Figure 1 before inducing experimental RM (except the sham). Animals were sacrificed, blood taken, and the kidneys harvested and homogenized. The total protein present in renal homogenates and isolated plasma were then precipitated and hydrolyzed to individual amino acids as described in the Materials and Methods section. Hydrolysates were then assessed for the content of 3-chlorotyrosine and unmodified tyrosine by quantitative mass spectrometry and finally expressed as **(A)** the ratio of 3-chlorotyrosine/tyrosine in the tissue. In some experiments, extracellular Mb was immunoprecipitated from the plasma and **(B)** the 3-chlorotyrosine/tyrosine ratio determined in the supernatant (RMIPS) and precipitate (RMIP). Data is expressed as a percentage of the maximum value measured in the RM group. Data represent mean ± SD; $n = 4$. *Different to the sham; $p < 0.01$. #Different to the corresponding level in the RM group; $p < 0.05$.

Se. These outcomes indicate that the AngII–ATRI/II axis may play a central role in promoting AKI following RM.

Others have reported that *di*phenyl-*di*selenide administered at ~7 mg/kg by oral gavage (equivalent to 7 ppm selenium) reverses AKI after RM (10). The mechanism of renal protection by *di*-phenyl-*di*selenide involves maintenance of low-molecular weight and proteinaceous antioxidants, although it is unclear whether urinary KIM-1, clusterin, or the renin–angiotensin pathway are affected by this form of dietary Se. Similarly, whether the renal tissue distribution of Se differs markedly when administered as selenite or *di*-phenyl-*di*selenide is not known. Notably, Se toxicity in rats occurs between 8–16 ppm in the diet (31), therefore simply increasing Se dose to enhance reno-protection must be approached with caution and exploring measures to improve bioavailability are warranted as a means to enhance reno-protection offered by dietary Se.

We recently assessed the efficacy of lipid- and water-soluble antioxidants in experimental RM and determined that water-soluble antioxidants were in general more effective than hydrophobic agents (23); however in this case the available data indicate the opposing view with increased reno-protection with *di*-phenyl-*di*selenide. Alternatively, our data suggest that selectively inhibiting AngII action on ERK/p38 and associated pathways that regulate NO bioavailability/activity may yield improved therapeutic approaches for treating AKI after RM.

Materials and Methods

Methods related to supplementary data are described in Supplementary Materials and Methods (available online at www.libertpub.com/ars).

Chemicals

Biochemicals were from Sigma Aldrich (Sydney, Australia), unless indicated otherwise. All chemicals were of the highest available quality. Antibodies for GPx-1, ATRI, and ATRII were from Abcam (Sydney, Australia), anti-SOD-1 (Sigma, MO) and anti-phospho ERK42/44 and p38 (Cell Signaling Technology, MA). The VECTASTAIN® ABC kit was from Vector Laboratories (CA). All buffers were prepared with MilliQ® Water.

Se supplementation

Male Sprague-Dawley rats (80–100 g) were from the Animal Resources Centre (Perth, Australia). Animals were acclimated for 2 weeks (body weights ranged 140 to 162 g), randomly assigned to groups, and provided a normal diet or sodium selenite supplemented diets *ad libitum*: 1 ppm (designated as Se+) or 5 ppm (Se++) prepared by Glen Forrest Specialty Feed (Perth, Western Australia). After 4-weeks of diet, animal weights did not differ significantly, although a trend to decreased weight was apparent in the Se++ group [normal chow 309 ± 18 g ($n = 15$); Se+ diet 292 ± 17 g ($n = 9$), and Se++ diet 285 ± 13 g ($n = 6$), mean ± SD]. Studies were conducted according to Local Ethics guidelines that adhered to NIH Guidelines for the Care and Use of Laboratory Animals.

Experimental rhabdomyolysis

Animals were dehydrated for 18 h before experimental RM as described previously (14, 15). Animals assigned to RM and Se-supplemented groups were anesthetized with isoflurane (2% v/v in $O_{2\ (g)}$, 1.5 l/min) then injected with 6 ml/kg of hypertonic glycerol (50% v/v in sterile saline) into each hind leg (this protocol yields RM with similar urinary Mb concentrations to levels determined after severe electrical burn in humans (32)). Animals in the sham group received an equal volume of sterile saline. Animals were then housed in metabolic cages with unrestricted access to chow/water and urine collected over 24 h.

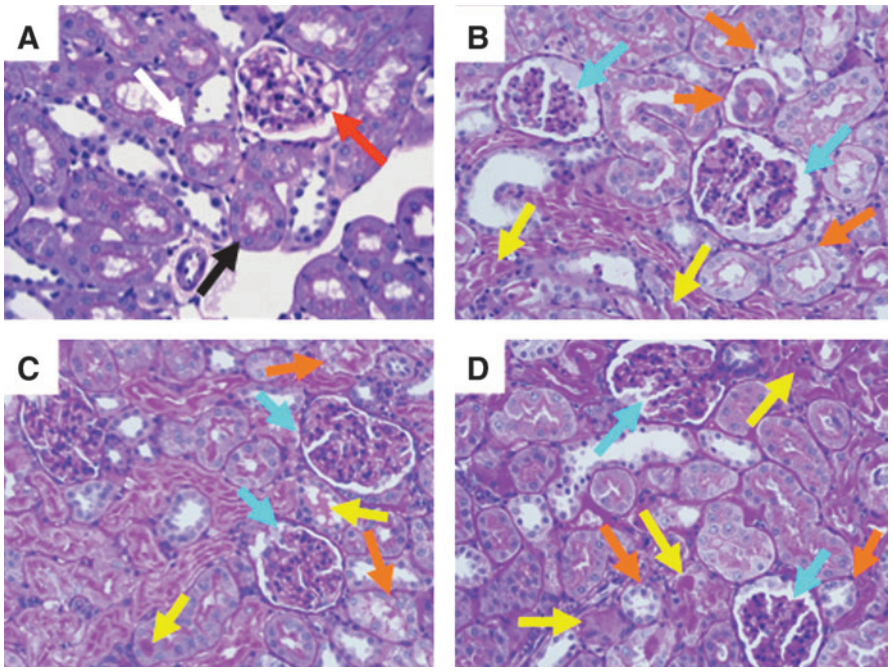

FIG. 6. Changes to renal architecture after experimental RM. Animals were treated as described in the legend to Figure 1 before inducing experimental RM (except the sham). After 24 h, the animals were euthanized and samples of kidney were isolated, embedded, sectioned, and stained with PAS. Representative sections are shown for **(A)** Sham, **(B)** RM, **(C)** Se+, and **(D)** Se++ treated rats. *Arrows* in **(A)** highlight unremarkable glomeruli in the renal cortex with thin walled capillaries in the glomerular tuft (*red arrow*); intact tubule epithelia (*black*) that are adherent to the tubule wall (*white*) in Sham tissues. *Arrows* in **(B–D)** highlight tubular casts (*yellow*), congested glomeruli with increased nuclear staining (*light blue*), necrotic tubular epithelial cells with some showing displacement from tubule (*orange*). Images are representative of 3 microscopic regions from $n = 3$–5 kidneys from different animals in the various treatment groups.

Harvest of blood and organs

Animals were anesthetized with isoflurane, followed by *i.p.* injection of ketamine (50 mg/kg weight) and xylazine (10 mg/kg weight). A thoracotomy was performed to expose the heart, and blood was collected via cardiac puncture (8–10 ml in 100 IU-heparin) and plasma was immediately isolated and stored at −80°C. Next the kidneys and aortae were harvested, the left kidney was sectioned, and the ventral portion was immersed in Tissue-Tek OCT (ProSciTech, Qld, Australia) and stored at −80°C for preparation of frozen sections. The remaining sample was stored in 4% v/v formalin for histological analysis. The right kidney was snap frozen in liquid nitrogen and stored at −80°C for subsequent molecular/biochemical analyses.

X-ray fluorescence microspectroscopy

Where required, kidneys were cryo-sectioned (30 μm) and mounted on to silicon nitride windows as described elsewhere (12), vacuum-sealed, and stored at 4°C prior to XFM. Elemental distribution maps of kidney sections were recorded on the X-ray fluorescence microspectroscopy (XFM) microprobe-beamline (39) at the Australian Synchrotron (Victoria,

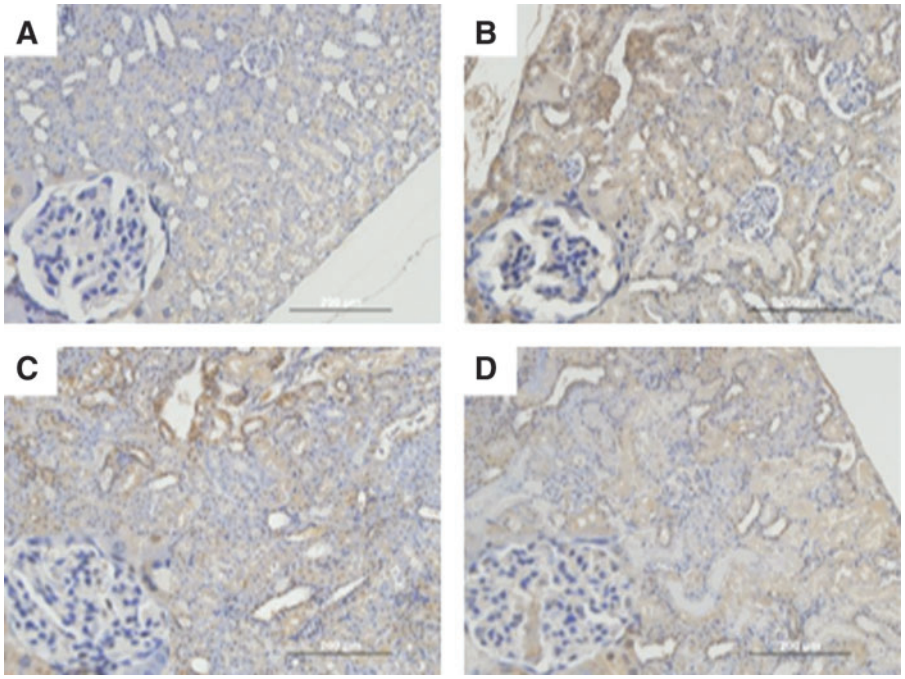

FIG. 7. Expression of Angiotensin II receptor 1 in renal tissues after experimental RM. Animals were treated as described in the legend to Figure 1 before inducing experimental RM (except the sham). After 24 h kidneys were harvested, fixed, embedded, sectioned, and stained. Panels show distribution of immunoactive ATRI accumulating in renal sections from **(A)** sham, **(B)** RM, **(C)** Se+, and **(D)** Se++ groups. Data are representative of several fields of view from $n = 3$ independent kidneys.

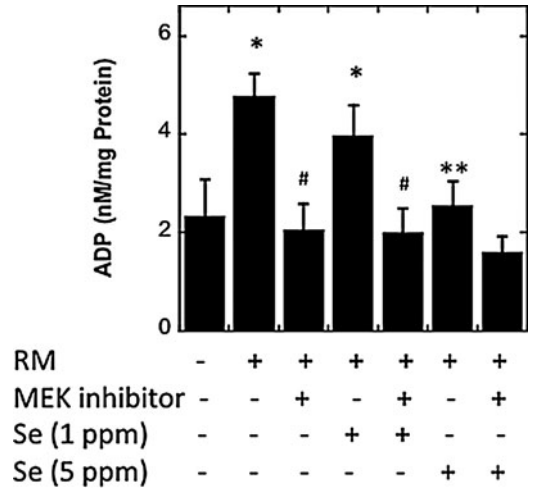

FIG. 8. Assessment of MAPK activity determined in renal tissues after experimental RM. Animals were treated as described in the legend to Figure 1 before inducing experimental RM (except the sham). After 24 h, the animals were euthanized and samples of kidney were isolated, homogenized, and MAPK activity was determined in the absence or presence of the MEK inhibitor (U0126) as described in Methods section. Data represents mean ± (SD); $n = 5$. *Different to the sham; $p < 0.05$. **Different to the RM group; $p < 0.05$. #Different to the corresponding group in the absence of U0126; $p < 0.01$.

Australia). A monochromatic 12.75 keV X-ray beam was focused (to a spot size of about $6 \times 2.5\ \mu$m) using a pair of horizontally- and vertically-focusing Kirkpatrick-Baez mirrors, and the fluorescence signal was collected using a single element silicon drift energy dispersive detector (Vortex EX, SII Nanotechnology, Northridge, CA), for 1 s per spatial point at a step size of 10 μm. As areas of interest were identified within the XFM images, higher resolution images were obtained from fluorescence signals collected for 2 s per spatial point at step size 2 μm.

Spectra for each spatial point was fit to Gaussians, modified by the addition of a step function and a tailing function to describe incomplete charge collection and other detector artifacts (19). Elemental contents (counts/s/pixel) were extracted from the fitted images. Further analysis was performed using MAPS software (61). Elemental content (counts/s/pixel) was normalized by X-ray scatter (counts/s/pixel) as a proxy for tissue thickness and therefore, the relative elemental contents are reported as dimensionless quantities.

Preparation of tissue homogenate

Intact frozen kidneys were thawed, diced, snap frozen in liquid nitrogen, pulverized to a fine powder, and homogenized for use in lipid analysis, enzyme activity assays, and gene response studies, as described previously (23, 32). Homogenate protein content was measured using the BCA assay (48).

Tissue and plasma lipid profile

Renal levels of UC, TOH, C18:2, C20:4, and CE-O(O)H were determined by high-performance liquid chromatography (48, 64). F_2-isoprostanes (nonenzymatic oxidation of arachidonic acid) were determined with an immunoassay kit (Cayman, Ann Arbor, MI; detection limit ~12 pmol/mg protein). All samples were saponified (10 *M* NaOH), neutralized (1 *M* HCl), centrifuged (3060 *g*), and the supernatant collected for isoprostane determinations. Finally, results were normalized to total homogenate protein.

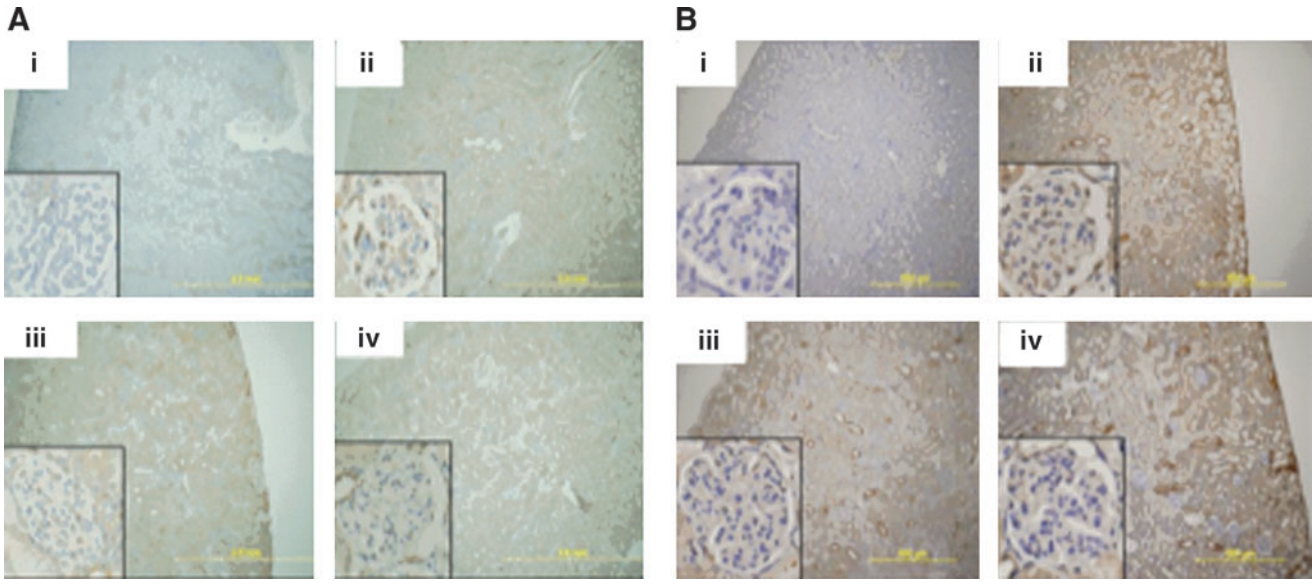

FIG. 9. Immunoactive phosphorylated ERK1/2 and p38 in rat kidney after experimental RM. Animals were treated as described in the legend to Figure 1 before inducing experimental RM (except the sham). After 24 h, animals were euthanized, kidneys harvested, fixed, and prepared for immunohistochemical analysis, as described in Methods section. Representative images show immunoactive **(A)** phosphorylated p38 and **(B)** phosphorylated ERK1/2 determined in (i) sham, (ii) RM, (iii) Se+, and (iv) Se++ treatment groups (inset 40X magnification of corresponding glomeruli). Data representative of at least 3 fields of view from $n = 3$ different kidneys.

Table 4. Primer Sequences for Q-PCR Analysis

Gene	*Forward primer*	*Reverse primer*	*Annealing temperature (°C)*
ATRI	5′-ATGCCAGTGTGTTTCTGCTC-3′	5′-CCAATGGGGAGTGTTGAGTT-3′	60°C
ATRII	5′-GTGTCCAGCATTTACATCTTCA-3′	5′-CACCAAACAAGGGGAACTAC-3′	60°C
β-ACTIN	5′-AGCCATGTACGTAGCCATCC-3′	5′-CTCTCAGCTGTGGTGGTGAA-3′	60°C
GPx-1	5′-TGAGAAGTGCGAGGTGAATG-3′	5′-AACACCGTCTGGACCTACCA-3′	60°C
NF-κB1	5′-TTCCCCACACTGTAAACCAA-3′	5′-AGCAAGTGTAATCCAATAGC-3′	60°C
SOD-1	5′-CCACTGCAGGACCTCATTTT-3′	5′-TCTTCATTTCCACCTTTGCC-3′	60°C
SOD-2	5′-GGCCAAGGGAGATGTTACAA-3′	5′-GCTTGATAGCCTCCAGCAAC-3′	60°C
TNFα	5′-AGGGTACCACAGAAAGATGC-3′	5′-GGAGATGAGACCCTTAGGTT-3′	58°C

Oligomers were synthesized by Sigma Aldrich (Sydney, Australia) and β-actin was employed as a housekeeping gene in all reverse transcriptase-PCR studies. The corresponding annealing temperatures employed in the RT-PCR reactions are also listed. ATRI/II, angiotensin receptors I and II; GPx-1, glutathione peroxidase-1; NFκB, nuclear factor kappa B; SOD-1/2, superoxide dismutase 1 and 2; TNF, tumor necrosis factor.

Assessment of tissue cGMP

Isolated aortae or renal tissues were thawed and homogenized in buffer containing the phosphodiesterase inhibitor 3-isobutyl-1-methyl-xanthine (100 μM, Sigma, MO) (23). Tissue cGMP was determined with a commercial ELISA kit (Cayman Chemical, MI) and normalized against renal homogenate protein.

Tissue gene response

Total RNA was extracted from renal homogenates with a kit (GeneElute; Sigma Aldrich, Sydney, Australia) and cDNA was constructed using BioScript Reverse Transcriptase (Bioline, Sydney, Australia) using a PCR-MasterCycler (Eppendorf, Sydney, Australia) (23, 32). Gene expression was determined by q-PCR, quantified by the comparative Ct method, normalized against β-actin, and expressed as fold-change relative to the sham using primer sequences shown in Table 4.

Renal antioxidant enzyme activity

Enzyme activity was determined using renal homogenates, and normalized against total protein (BCA Assay; Sigma, Sydney, Australia). The homogenized tissue was centrifuged (5000 g, 5 min) and the supernatant further clarified (5000 g, 5 min) and collected for enzyme activity assays. Total SOD activity was measured as described previously (2). Glutathione peroxidase activity was analyzed by monitoring NADPH consumption with H_2O_2 as the cofactor (63).

Western blot analysis

Renal homogenates were normalized to total protein, loaded onto SDS-PAGE, then transferred to nitrocellulose for Western blotting. Antibodies against GPx-1 (Sigma, Australia), β-actin (loading control; Sigma) and p-(serine 276)P65 (Signalway, MD) were employed.

Kidney histology

Kidney sections were de-paraffinized, rehydrated, and thin sections (5 μm) were treated with periodic acid and stained in Schiff's reagent, counterstained with Mayer's hematoxylin, dehydrated, and mounted with DPX solution, as described previously (41).

Immunohistochemistry

Thin sections (5 μm) were cut and mounted onto SuperFrost Plus slides for staining using a Dako Auto-immunostainer. Sections were de-paraffinized, blocked with 3% v/v albumin in TBS-T and 5% v/v goat serum, then incubated with the appropriate primary antibody (dilution 1:200 v/v, 60 min). Controls were incubated with TBS-T (negative control). All sections were washed and incubated with a biotin-conjugated secondary antibody (1:250 v/v, 30 min, Vectastain ABC). Samples treated with secondary antibody alone or TBS-T acted as negative controls. Sections were washed, incubated with streptavidin-conjugated HRP (1:250 v/v, 30 min, Vectastain ABC) and visualized with DAB (DAKO, Sydney Australia). Sections were counterstained with Mayer's hematoxylin, dehydrated, and mounted using DPX solution (DAKO). Images were captured with an Olympus Microscope using a digital camera (DP Controller; v2.2.1.227) and converted to TIFF for handling with MS PowerPoint (2008, v7).

Inflammatory marker CCL2/MCP-1

The pro-inflammatory chemokine MCP-1 was analyzed in samples of plasma and renal homogenates using a commercial AlphaLISA® CCL2 / MCP1 Kit, following the manufacturer's instructions and using a Pherastar Microplate Reader with AlphaScreen standard settings.

Markers for acute kidney injury

Glomerular filtration rate. Plasma and urinary levels of Na^+, K^+, Cl^-, Ca^{2+}, creatinine, and total protein were determined by the Diagnostic Pathology Unit (Concord Hospital, Sydney Australia). Serum and urinary creatinine levels were used to calculate CCr, as we reported previously (23, 32).

Urinary markers. Urinary clusterin, KIM-1, and osteopontin were analyzed using a MILLIPLEX Kidney Toxicity Panel (Millipore, Sydney, Australia) and a Luminex® xMAP® multiplex platform.

Kinase activity assay

An ADP-Glo™ Kinase Assay (Promega, WI) was used to analyze MAPK activity in renal homogenates using phospholipase A2 (a specific substrate for ERK). Where required, MAPK activity was inhibited by addition of the MEK1/2 inhibitor (U0126–IC50 of 72 nM for MEK1 and 58 nM for MEK2;

Sigma). Plates were read using a Pherastar Microplate Reader and exported to Microsoft Excel (v7) for further manipulation.

Assessment of renal 3-chloro-tyrosine levels

Renal homogenates were delipidated and precipitated by the addition of 3% w/v sodium deoxycholate and 50% w/v trichloroacetic acid prior to centrifugation at (6000 $g \times 5$ min). Pellets were washed with acetone, centrifuged (6000 $g \times 5$ min) to remove acetone, dried under a stream of $N_{2(g)}$, resuspended in 6 *M* methanesulfonic acid containing 0.2% tryptamine, and finally hydrolyzed under vacuum at 110°C for ~12 h, as described previously (27).

Detection and quantification of 3-chlorotyrosine (3-Cl-Tyr) was performed by quantitative mass spectrometry (54). Briefly, 3-chloro-[13C9,15N] tyrosine and [15N]-tyrosine (final concentration 1.5 nmol) were added to each sample as an internal standards before hydrolysis, using the protocol outlined above. The hydrolysates were purified using solid-phase extraction columns (Supelco, Sydney, Australia) that were activated with 100% methanol before preconditioning (2×2 ml) using 0.1% TFA/H_2O. Samples were loaded and washed on the columns with 2 ml of 0.1% v/v TFA/H_2O and eluted with 80% v/v methanol/H_2O, dried under vacuum at 60°C, and re-dissolved in 100 μl of 0.1% v/v formic acid. Unmodified tyrosine and 3-Cl-Tyr were detected using an Agilent LC-MS and quantified using an external calibration curve that was constructed with authentic Tyr and 3-Cl-tyr and their corresponding isotopically labeled forms (0–500 pmol). The peak area for each Tyr residue relative to its internal standard was then employed in determinations of the ratio of the 3-Cl-tyr/Tyr ratio.

Statistical analysis

Statistical analysis was performed using GraphPad Prism (Version 5.00 for Windows), and data were evaluated using one-way ANOVA with Newman-Keuls post-hoc test for multiple comparisons; significance was accepted at the 95% confidence level ($p < 0.05$).

Acknowledgments

We thank the support from the Australian Research Council [Discovery DP0878559 Grant to PKW, DP0985807 to HHH and PKW, and Lief grant LE100100125] and the Bosch Molecular Biology Facility for access to the Luminex200 platform. Portions of this research were performed at the XFM beamline at the Australian Synchrotron.

Author Disclosure Statement

No competing financial interests exist.

References

1. Agay D, Sandre C, Roussel AM, and Chancerelle Y. Optimization of selenium status by a single intraperitoneal injection of Se in Se-deficient rat: Possible application to burned patient treatment. *Free Radic Biol Med* 39: 762–768, 2005.
2. Ahmed H, Schott EJ, Gauthier JD, and Vasta GR. Superoxide dismutases from the oyster parasite *Perkinsus marinus*: Purification, biochemical characterization, and development of a plate microassay for activity. *Anal Biochem* 318; 132–141, 2003.
3. Andriambeloson E and Witting PK. Chemical regulation of nitric oxide: A role for intracellular myoglobin? *Redox Rep* 7; 131–136, 2002.
4. Ashton K, Hooper L, Harvey LJ, Hurst R, Casgrain A, and Fairweather-Tait SJ. Methods of assessment of selenium status in humans: A systematic review. *Am J Clin Nutr* 89; 2025S–2039S, 2009.
5. Aydogdu N, Atmaca G, Yalcin O, Batcioglu K, and Kaymak K. Effects of caffeic acid phenethyl ester on glycerol-induced acute renal failure in rats. *Clin Exp Pharmacol Physiol* 31; 575–579, 2004.
6. Bagshaw SM, Bellomo R, Devarajan P, Johnson C, Karvellas CJ, Kutsiogiannis DJ, Mehta R, Pannu N, Romanovsky A, Sheinfeld G, Taylor S, Zappitelli M, and Gibney RT. Acute kidney injury in critical illness. *Can J Anesth* 57; 985–998, 2010.
7. Banday AA and Lokhandwala MF. Oxidative stress causes renal angiotensin II type 1 receptor upregulation, Na_/H_ exchanger 3 overstimulation, and hypertension. *Hypertension* 57; 452–459, 2011.
8. Bosch X, Poch E, and Grau JM. Rhabdomyolysis and acute kidney injury. *N. Engl. J. Med*. 361; 62–72, 2009.
9. Boutaud O and Roberts LJ. Mechanism based therapeutic approaches to rhabdomyolysis-induced renal failure. *Free Radic Biol Med* 51; 1062–1067, 2011.
10. Brandão R, Acker CI, Leite MR, Barbosa NB, and Nogueira CW. Diphenyl diselenide protects against glycerol-induced renal damage in rats. *J Appl Toxicol* 29; 612–618, 2009.
11. Caldeira C, Neves WS, Cury PM, Serrano P, Baptista MA, and Burdmann EA. Rhabdomyolysis, acute renal failure, and death after monensin ingestion. *Am J Kidney Dis* 38; 1108–1112, 2001.
12. Carter EA, Rayner BS, McLeod AI, Wu LE, Marshall CP, Levina A, Aitken JB, Witting PK, Lai B, Cai Z, Vogt S, Lee YC, Chen CI, Tobin MJ, Harris HH, and Lay PA. Silicon nitride as a versatile growth substrate for microspectroscopic imaging and mapping of individual cells. *Mol Biosyst* 6; 1316–1322, 2010.
13. Chandel NS., Trzyna WC, McClintock DS, and Schumacker PT. Role of oxidants in NF-κB activation and TNF-α gene transcription induced by hypoxia and endotoxin. *J Immunol* 165; 1013–1021, 2000.
14. Chander V, Singh D, and Chopra K. Reversal of experimental myoglobinuric acute renal failure in rats by quercetin, a bioflavonoid. *Pharmacology* 73; 49–56, 2005.
15. Chander V and Chopra K. Protective effect of resveratrol, a polyphenolic phytoalexinon glycerol-induced acute renal failure in rat kidney. *Renal Failure* 28; 161–169, 2006.
16. Chatzizisis YS, Misirli G, Hatzitolios AI, and Giannoglou GD. The syndrome of rhabdomyolysis: Complications and treatment. *Eur J Intern Med* 19; 568–574, 2008.
17. Domigan NM, Charlton TS, Duncan MW, Winterbourn CC, and Kettle AJ. Chlorination of tyrosyl residues in peptides by myeloperoxidase and human neutrophils. *J Biol Chem* 270; 16542–16548, 1995.
18. Duhm J and Göbel BO. Na+-K+ transport and volume of rat erythrocytes under dietary K+ deficiency. *Am J Physiol* 246; C20–29, 1984.
19. Espen PV. Spectrum Evaluation. In: *Handbook of X-Ray Spectrometry: Second Edition: Revised and Expanded;* Grieken REV and Markowicz AA, eds. Marcel Dekker, Inc., New York. 2002.
20. Grisham MB. Myoglobin-catalyzed hydrogen peroxide dependent arachidonic acid peroxidation. *J Free Radic Biol Med* 1; 227–232, 1985.

21. Galla JH, Bonduris DN, Kirk KA, and Luke RG. Effect of dietary NaCl on chloride uptake in rat collecting duct segment. *Am J Physiol* 251; F454–F459, 1986.
22. Groebler LK, Liu J, Shanu A, Codd R, and Witting PK. Comparing the potential renal protective activity of desferrioxamine B and the novel chelator desferrioxamine B-N-(3-hydroxy-adamant- 1-yl)carboxamide in a cell model of myoglobinuria. *Biochem J* 435; 669–677, 2011.
23. Groebler LK, Kim HB, Shanu A, Hossain F, McMahon AC, and Witting PK. Co-supplementation with a synthetic polyphenol and vitamin C inhibits oxidative damage and improves vascular function yet does not inhibit acute renal injury in an animal model of rhabdomyolysis. *Free Radic Biol Med* 52; 1918–1928, 2012.
24. Hamaguchi A, Kim S, Yano M, Yamanaka S, and Iwao H. Activation of glomerular mitogen-activated protein kinases in angiotensin II-mediated hypertension. *J Am Soc Nephrol* 9; 372–380, 1998.
25. Harrison-Bernard LM. The renal renin-angiotensin system. *Adv Physiol.Educ* 33; 270–274, 2009.
26. Hazen SL and Heinecke JW. 3-Chlorotyrosine, a specific marker of myeloperoxidase-catalyzed oxidation, is markedly elevated in low-density lipoprotein isolated from human atherosclerotic intima. *J Clin Invest* 99; 2075–2081, 1997.
27. Hawkins CL, Morgan PE, and Davies MJ. Quantification of protein modification by oxidants. *Free Rad Biol Med* 46; 965–988; 2009.
28. Hidaka S, Kränzlin B, Gretz N, and Witzgall R. Urinary clusterin levels in the rat correlate with the severity of tubular damage and may help to differentiate between glomerular and tubular injuries. *Cell Tissue Res* 310; 289–296, 2002.
29. Hii CS, Huang ZH, Bilney A, Costabile M, Murray AW, Rathjen DA, Der CJ, and Ferrante A. Stimulation of p38 phosphorylation and activity by arachidonic acid in HeLa cells, HL60 promyelocytic leukemic cells, and human neutrophils. Evidence for cell type-specific activation of mitogen-activated protein kinases. *J Biol Chem* 273; 19277–19282, 1998.
30. Holt SG and Moore KP. Pathogenesis and treatment of renal dysfunction in rhabdomyolysis. *Intensive Care Med* 27; 803–811, 2001.
31. Jacobs M and Forst C. Toxicological effects of sodium selenite in Sprague-Dawley rats. *J Toxicol Environ Health* 8; 575–585, 1981.
32. Kim HB, Shanu A, Wood S, Parry SN, Collet M, McMahon AC, and Witting PK. Phenolic antioxidants tert-butylbisphenol and Vitamin E decrease oxidative stress and enhance vascular function in an animal model of rhabdomyolysis yet do not improve acute renal dysfunction. *Free Rad Res* 45; 1000–1012, 2011.
33. Kim JH, Gil HW, Yang JO, Lee EY, and Hong SY. Serum uric acid level as a marker for mortality and acute kidney injury in patients with acute paraquat intoxication. *Nephrol Dial Transplant* 26; 1846–1852, 2011.
34. Malinouski M, Kehr S, Finney L, Vogt S, Carlson BA, Seravalli J, Jin R, Handy DE, Park TJ, Loscalzo J, Hatfield DL, and Gladyshev VN. High-resolution imaging of selenium in kidneys: A localized selenium pool associated with glutathione peroxidase. *Antioxid Redox Signal* 16; 185–192, 2012.
35. Manitius A, Levitin H, Beck D, and Epstein FH. On the mechanism of impairment of renal concentrating ability in hypercalcemia. *J Clin Invest* 39; 693–697,1960.
36. Olsson U and Kallner A. Effects of starvation and of selenium deficiency on the urinary excretion of electrolytes, ketone bodies, creatinine, urea and uric acid. *J Trace Elem Med Biol* 9; 88–93, 1995.
37. Paller MS. Hemoglobin-and myoglobin-induced acute renal failure in rats: Role of iron in nephrotoxicity. *Am J Physiol* 255; F539– 544, 1988.
38. Palmieri T, Lavrentieva A, and Greenhalgh DG. Acute kidney injury in critically ill burn patients. Risk factors, progression and impact on mortality. *Burns* 36; 205–211, 2010.
39. Paterson D, de Jonge MD, Howard DL, Lewis W, McKinlay J, Starritt A, Kusel M, Ryan CG, Kirkham R, Moorhead G, and Siddons, DP. The X-ray fluorescence microscopy beamline at the Australian Synchrotron. *AIP Conf Proc* 1365; 219–222, 2011.
40. Plotnikov EY, Chupyrkina AA, Jankauskas SS, Pevzner IB, Silachev DN, Skulachev VP, and Zorov DB. Mechanisms of nephroprotective effect of mitochondria-targeted antioxidants under rhabdomyolysis and ischemia/reperfusion. *Biochim Biophys Acta* 1812; 77–86, 2011.
41. Ponraj D and Gopalakrishnakone P. Renal lesions in rhabdomyolysis caused by *Pseudechis australis* snake myotoxin. *Kidney Int* 51; 1956–1969, 1997.
42. Rayman MP. The importance of selenium to human health. *Lancet* 356; 233–241, 2000.
43. Rayner BS, Wu BJ, Raftery M, Stocker R, and Witting PK. Human S-nitroso oxymyoglobin is a store of vasoactive nitric oxide. *J Biol Chem* 280; 9985–9993, 2005.
44. Reeder BJ and Wilson MT. Hemoglobin and myoglobin associated oxidative stress: From molecular mechanisms to disease states. *Curr Med Chem* 12; 2741–2751, 2005.
45. Rosenberg ME and Silkensen J. Clusterin: Physiologic and pathophysiologic considerations. *Int J Biochem Cell Biol.* 27; 633–645, 1995.
46. Ruiz-Ortega M, Bustos C, Hernández-Presa MA, Lorenzo O, Plaza JJ, and Egido J. Angiotensin II participates in mononuclear cell recruitment in experimental immune complex nephritis through nuclear factor-kappa B activation and monocyte chemoattractant protein-1 synthesis. *J Immunol* 161; 430–439, 1998.
47. Sandre C, Agay D, Ducros V, Faure H, Cruz C, Alonso A, Chancerelle Y, and Roussel AM. Kinetic changes of oxidative stress and selenium status in plasma and tissues following burn injury in selenium-deficient and selenium-supplemented rats. *J Trauma* 60; 627–634, 2006.
48. Sattler W, Mohr D, and Stocker R. Rapid isolation of lipoproteins and assessment of their peroxidation by high performance liquid chromatography post-column luminescence. *Methods Enzymol* 233; 469–489, 1994.
49. Shanu A, Parry SN, Wood S, Rodas E, and Witting PK. The synthetic polyphenol tert-butyl-bisphenol inhibits myoglobin-induced dysfunction in cultured kidney epithelial cells. *Free Rad Res* 44; 843–853, 2010.
50. Stollwerck PL, Namdar T, Stang FH, Lange T, Mailänder P, and Siemers F. Rhabdomyolysis and acute renal failure in severely burned patients. *Burns* 37; 240–248, 2011.
51. Sunde RA, Raines AM, Barnes KM, and Evenson JK. Selenium status highly regulates selenoprotein mRNA levels for only a subset of the selenoproteins in the selenoproteome. *Biosci Rep* 29; 329–338, 2009.
52. Szuchman-Sapir AJ, Pattison DI, Davies MJ, and Witting PK. Site-specific hypochlorous acid-induced oxidation of recombinant human myoglobin affects specific amino acid residues and the rate of cytochrome b5-mediated heme reduction. *Free Radic Biol Med* 48; 35–46, 2010.

53. Takahashi M, Suzuki E, Takeda R, Oba S, Nishimatsu H, Kimura K, Nagano T, Nagai R, and Hirata Y. Angiotensin II and tumor necrosis factor-alpha synergistically promote monocyte chemoattractant protein-1 expression: Roles of NF-kappaB, p38, and reactive oxygen species. *Am J Physiol Heart Circ Physiol* 294; H2879–2888, 2008.
54. Talib J, Pattison DI, Harmer JA, Celermajer DS, and Davies MJ. High plasma thiocyanate levels modulate protein damage induced by myeloperoxidase and perturb measurement of 3-chlorotyrosine. *Free Radic Biol Med* 53; 20–29; 2012.
55. Tanifuji C, Suzuki Y, Geot WM, Horikoshi S, Sugaya T, Ruiz-Ortega M, Egido J, and Tomino Y. Reactive oxygen species-mediated signaling pathways in angiotensin II-induced MCP-1 expression of proximal tubular cells. *Antioxid Redox Signal* 7; 1261–1268, 2005.
56. Thomas SR, Witting PK, and Drummond GR. Redox control of endothelial function and dysfunction: Molecular mechanisms and therapeutic opportunities. *Antioxid Redox Signal* 10; 1713–1765, 2008.
57. Toque HA, Romero MJ, Tostes RC, Shatanawi A, Chandra S, Carneiro ZN, Inscho EW, Webb RC, Caldwell RB, and Caldwell RW. p38 Mitogen-activated protein kinase (MAPK) increases arginase activity and contributes to endothelial dysfunction in corpora cavernosa from angiotensin-II-treated mice. *J Sex Med* 7; 3857–3867, 2010.
58. Ustundag S, Yalcin O, Sen S, Cukur Z, Ciftci S, and Demirkan B. Experimental myoglobinuric acute renal failure: The effect of vitamin C. *Renal Failure* 30; 727–735, 2008.
59. Vaidya VS, Ferguson MA, and Bonventre JV. Biomarkers of acute kidney injury. *An Rev Pharmacol Toxicol* 48; 463–493, 2008.
60. Venardos KM, Perkins A, Headrick J, and Kaye DM. Myocardial ischemia-reperfusion injury, antioxidant enzyme systems, and selenium: A review. *Curr Med Chem* 14; 1539–1549, 2007.
61. Vogt SJ. MAPS. A set of software tools for analysis and visualization of 3D X-ray fluorescence data sets. *Phys IV* 104; 635–638, 2003.
62. Waanders F, van Timmeren MM, Stegeman CA, Bakker SJ, and van Goor H. Kidney injury molecule-1 in renal disease. *J Pathol* 220; 7–16, 2010.
63. Wilson SR, Zucker PA, Huang RRC, and Spector A. Development of synthetic compounds with glutathione peroxidase activity. *J Am Chem Soc* 111: 5936–5939, 1989.
64. Witting P, Pettersson K, Ostlund-Lindqvist AM, Westerlund C, Wâgberg M, aand Stocker R. Dissociation of atherogenesis from aortic accumulation of lipid hydro (per)oxides in Watanabe heritable hyperlipidemic rabbits. *J Clin Invest* 104: 213–220, 1999.
65. Zager RA. Studies of mechanisms and protective maneuvers in myoglobinuric acute renal injury. *Lab Invest* 60: 619–629, 1989.

Address correspondence to:
Dr. Paul Witting
Discipline of Pathology
Redox Biology Group, Room W503
Bosch Institute
Balckburn Building D06
The University of Sydney
Sydney
New South Wales 2006
Australia

E-mail: paul.witting@sydney.edu.au

Date of first submission to ARS Central, February 28, 2012; date of final revised submission, August 28, 2012; date of acceptance, September 2, 2012.

Abbreviations Used

AKI = acute kidney injury
AngII = angiotensin II
ATRI = angiotensin receptor I
ATRII = angiotensin receptor II
BUN = blood urea nitrogen
CE = cholesteryl ester
CE-O(O)H = cholesteryl ester derived lipid hydroperoxides and hydroxides
CCr = creatinine clearance
cGMP = cyclic guanosine monophosphate
ERK = extracellular-signal related kinase
GPx = glutathione peroxidase
KIM-1 = kidney-injury-molecule I
MAP kinase = mitogen-activated protein kinase
Mb = myoglobin
MCP-1 = monocyte chemoattractant protein I
NFκB = nuclear factor kappa beta
NO = nitric oxide
*p*NPP = p-nitrophenyl phosphate
RM = rhabdomyolysis
Se = selenium
SOD1/2 = superoxide dismutase 1/2
TNF = tumor necrosis factor
TOH = tocopherol
UC = unesterified cholesterol
XFM = X-ray fluorescence microscopy